Adsorption and photocatalytic oxidation of ibuprofen using nanocomposites of TiO2 nanofibers combined with BN nanosheets: Degradation products and mechanisms

Lu Lin, Wenbin Jiang, Mikhael Bechelany, Maryline Nasr, Jacqueline Jarvis, Tanner Schaub, Rishi Sapkota, Philippe Miele, Huiyao Wang, Pei Xu

Adsorption and photocatalytic oxidation of ibuprofen using nanocomposites of TiO_2 nanofibers combined with BN nanosheets: degradation products and mechanisms

Lu Lin[1], Wenbin Jiang[1], Mikhael Bechelany[2], Maryline Nasr[2], Jacqueline Jarvis[3], Tanner Schaub[3], Rishi R. Sapkota[3], Philippe Miele[2], Huiyao Wang[4*], Pei Xu[1*]

[1]Department of Civil Engineering, New Mexico State University, 3035 S Espina Street, Las Cruces, NM 88003, USA

[2]Institut Européen des Membranes, IEM, UMR-5635, Université de Montpellier, ENSCM, CNRS, Place Eugène Bataillon, F-34095 Montpellier Cedex 5, France

[3]Chemical Analysis and Instrumentation Laboratory, College of Agricultural, Consumer and Environmental Sciences, New Mexico State University, Las Cruces, NM 88003, USA

[4]Core University Research Resources Laboratory, New Mexico State University, Las Cruces, NM 88003, USA

[*]Corresponding author: Dr. Huiyao Wang, Email: huiyao@nmsu.edu

[*]Corresponding author: Dr. Pei Xu, Email: pxu@nmsu.edu

Abstract

This study investigated the adsorption and photocatalytic activity of TiO_2-boron nitride (BN) nanocomposites for the removal of contaminants of emerging concern in water using ibuprofen as a model compound. TiO_2 nanofibers wrapped by BN nanosheets were synthesized by electrospinning method. Characterization of the nanocomposite photocatalysts indicated the BN nanosheets improved the light absorbance and reduced the recombination of the photoexcited charge carriers (e^- and h^+). The photocatalytic oxidation products and mechanisms of ibuprofen by the TiO_2-BN catalysts were elucidated using a multiple analysis approach by high performance liquid chromatography, ultraviolet absorbance, dissolved organic carbon, fluorescence excitation-emission matrices, and electrospray ionization–liquid chromatography–tandem mass spectrometry. The experimental results revealed that the photocatalytic oxidation by the TiO_2-BN nanocomposites is a multi-step process and the interactions between ibuprofen molecules and the TiO_2-BN nanocomposites govern the adsorption process. The increasing BN nanosheet content in the TiO_2 nanofibers facilitated the breakdown of ibuprofen degradation intermediates (hydroxyibuprofen, carboxyibuprofen, and oxypropyl ibuprofen). Kinetic modeling indicated both adsorption and photocatalytic oxidation of ibuprofen by the TiO_2-BN nanocomposites followed the first-order kinetic model. The photocatalytic oxidation rate increased with the increasing BN content in the nanocomposite catalysts, which was attributed to the light absorption capacity and the separation efficiency of the photoexcited electron (e^-)-hole (h^+) pairs. Multiple photocatalytic cycles were conducted to investigate the reusability and regeneration of the nanofibers for degradation of ibuprofen.

Keywords: titanium dioxide boron-nitride nanocomposites; photocatalytic oxidation; adsorption; degradation intermediates; photocatalytic degradation mechanisms

1. Introduction

Contaminants of emerging concerns such as pharmaceuticals and personal care products (PPCPs) have been widely detected in water bodies around the world (Vieno et al., 2007). Many PPCPs are of serious concerns even in trace amounts due to their toxicity to aquatic life and potential risks to public health (Vieno et al., 2007; Christen et al., 2010). Conventional water and wastewater treatment processes including coagulation, sedimentation, media filtration, and biological processes are not effective to remove these recalcitrant organic contaminants (Vieno et al., 2007; Xiang et al., 2016). Adsorption by activated carbon is an efficient technique to remove hydrophobic PPCPs through hydrophobic interactions, however the adsorption capacity gradually decreases as the carbon is saturated with the adsorbed chemicals. In addition, it is ineffective to adsorb hydrophilic compounds such as atenolol, acetaminophen, and naproxen (Vieno et al., 2007; Huerta-Fontela et al., 2011; Wang et al., 2015). Oxidation using chlorine, chlorine dioxide, and ozone is typically effective to degrade PPCPs with electron-donating functional groups (e.g., phenolic-and amine-containing compounds) (Lee and von Gunten, 2010). Ultraviolet (UV) irradiation can degrade many PPCPs but treatment cost is inhibitive because of high energy demand (Rosenfeldt and Linden, 2004).

To degrade the persistent organic contaminants, advanced oxidation processes (AOPs) are typically needed (De la Cruz et al., 2012). AOPs generate hydroxyl radicals (·OH) which react non-selectively with most organic compounds (Andreozzi et al., 1999). Commonly used AOPs for PPCPs removal from wastewater include UV/H_2O_2, UV/O_3, (photo)-Fenton, and heterogeneous photocatalysis (De Witte et al., 2009; Homem and Santos, 2011; Prieto-Rodriguez et al., 2012; Carbonaro et al., 2013; Van Doorslaer et al., 2015; Thagard et al., 2016). Complete mineralization is usually not the goal of AOPs because it is energy intensive and not cost-

effective (Doll and Frimmel, 2004). Partial degradation of recalcitrant PPCPs is more economically attractive to deactivate their biological activity or increase their biodegradability (Van Doorslaer et al., 2015). But more concerns are raised regarding the intermediate degradation products and their environmental toxicities.

Heterogeneous photocatalytic oxidation using metal oxides (e.g., TiO_2) has attracted considerable attention particularly due to its potentially lower cost than other AOPs (Jing et al., 2006; Dalrymple et al., 2007; Rubio et al., 2013; Lin et al., 2015; Arlos et al., 2016; Lin et al., 2016; Lin et al., 2017b; Lin et al., 2017f; Li and Hu, 2018). More than 90 organic and 25 inorganic compounds catalogued on the US Environmental Protection Agency's (USEPA) priority list of contaminants have been investigated using heterogeneous photocatalysis (Blake, 2001), such as acetone, aniline, atrazine, benzene, methyl tertiary butyl ether (MTBE), trichloroethane. The process has also been successfully applied for the treatment of organic and inorganic compounds at low concentrations in aqueous solutions (Wold, 1993; Nakajima et al., 2005; Westerhoff et al., 2005; Le-Clech et al., 2006).

During heterogeneous photocatalysis, organic molecules adsorb onto a metal oxide catalyst surface and react with the photoexcited charge carriers (e^- and h^+) or free radicals (e.g., ·OH) (Ollis et al., 1984; Kormann et al., 1991). The photocatalytic reaction depends on the species of organic molecules adsorbed onto the photocatalyst surface and in aqueous phase, which results in different kinetics of photodegradation. As a critical step in heterogeneous photocatalysis, very few studies investigated the kinetics of organics adsorption on a photocatalyst (Bauer et al., 2001; Vautier et al., 2001; Hu et al., 2003; Yu et al., 2005; Lee et al., 2011; Zhang et al., 2013; Rioja et al., 2014; Lv et al., 2016).

89 Titanium dioxide (TiO_2) is the most commonly used photocatalyst due to its relatively low cost,
90 high stability, and low toxicity (Fujishima et al., 2000; Kumar and Devi, 2011a; Nakata and
91 Fujishima, 2012). Substantial efforts have been devoted to improve the photocatalytic
92 degradation efficiency of TiO_2 through combination with metal ions, non-metal ions, and some
93 2D nanomaterials (Liqiang et al., 2006; Rubio et al., 2013; Lin et al., 2015; Arlos et al., 2016;
94 Lin et al., 2016; Lin et al., 2017b; Lin et al., 2017f; Li and Hu, 2018; Yi et al., 2018; Merenda et
95 al., 2019). These dopants, such as Ag (Harifi and Montazer, 2014), Fe (Asiltürk et al., 2009; Lin
96 et al., 2016), P (Zhang et al., 2012), SiO_2 (Tawkaew and Supothina, 2008), and graphene (oxide)
97 (Lin et al., 2017c; Lin et al., 2017d; Yi et al., 2018), have been proven to be effective to improve
98 the photocatalytic activity. A recent study reported that the boron nitride (BN) nanosheets exhibit
99 unique properties due to the high surface area and the reactive edge structure (Biscarat et al.,
100 2015). Previous study demonstrated that the introduction of BN nanosheets enhanced the
101 separation of electron–hole pairs of TiO_2 and dramatically improved photocatalytic activity of
102 methyl orange under ultraviolet (UV) irradiation (Nasr et al., 2017b).

103 This study aims to investigate the mechanisms and kinetics of adsorption and photocatalytic
104 oxidation of PPCPs using novel photocatalytic composite TiO_2 nanofibers with boron nitride
105 (BN) nanosheets. Combining TiO_2 with BN nanosheets by electrospinning method is anticipated
106 to enhance the separation of e^--h^+ pairs of TiO_2 thus to improve the photocatalytic activity.
107 Ibuprofen, a nonsteroidal anti-inflammatory drug that has been found extensively in wastewater
108 effluents, was used as the target recalcitrant PPCP. The adsorption and degradation of ibuprofen
109 by photolysis and photocatalysis was characterized by a series of analytical methods.
110 Degradation intermediates of ibuprofen were analyzed by a positive ion electrospray ionization–
111 liquid chromatography–tandem mass spectrometry [(+) ESI LC-MS/MS]. Multiple

112 photocatalytic cycles were conducted to evaluate the recyclability and regeneration of the TiO_2-
113 BN nanocomposites for the degradation of ibuprofen.

114

115 **2. Materials and methods**

116 2.1 Materials and characterization

117 A series of BN nanosheets incorporated TiO_2 nanofibers (0, 3%, 5%, 7%, and 10%, weight
118 percentage of BN to the mass of Ti, referred as TiO_2, TB1, TB2, TB3, and TB4, respectively)
119 were synthesized using electrospinning technique as described by Nasr et al. (2017b). UV-Vis
120 absorbance of the nanofibers was measured by a spectrophotometer (DR6000; Hach Company,
121 CO). X-ray diffraction (XRD) measurements were conducted using a PANAlytical Xpert-PRO
122 diffractometer equipped with an X'celerator detector using Ni-filtered Cu-radiation. The specific
123 surface area of the nanocomposites was determined from the nitrogen adsorption–desorption
124 isotherms measured at liquid nitrogen temperature using a Micromeritics ASAP 2010
125 (outgassing conditions: 200 ^{o}C and 12 h). The structure and morphology of the nanocomposite
126 catalysts was characterized by an H-7650 transmission electron microscope (TEM; Hitachi High-
127 Technologies Corp., Pleasanton, CA). The elemental mapping images were taken with a Zeiss
128 EVO HD15 microscope coupled with an Oxford X-MaxN EDX detector.

129

130 2.2 Adsorption and photodegradation experiments

131 Ibuprofen (Analytical grade; Acros Organics Co, NJ) was used as a model compound
132 representative of PPCPs to evaluate the adsorption and photocatalytic activity of the synthesized
133 nanocomposites. The pH of the tested ibuprofen solution was neutral throughout the experiments.

Batch experiments were conducted in 100 mL beakers containing a suspension of 10 mg nanofibers and 50 mL ibuprofen solution (5 mg L^{-1}) under dark (adsorption), UV light irradiation with nanofibers (photocatalysis) or without nanofibers (photolysis) conditions. The irradiance of UV lamp (160W PUV-10, Zoo Med Laboratories, San Luis Obispo, CA) included both UV (365 nm, minor peaks at 290, 315, 335 nm) and visible light (405, 435, and 545 nm) wavelength spectrum. The solution mixtures were magnetically stirred for 2 to 3 hours, and 1 mL water samples were taken at 0, 10, 20, 30, 60, 90, 120, and 180 min. The suspensions were then filtered through 0.45 μm cellulose acetate membrane to separate nanofibers for analysis. All adsorption, photolysis, and photocatalytic degradation experiments under each condition were conducted at least two times to ensure the reproducibility of the results.

Repeated ibuprofen degradation experiments were conducted for 16 cycles to evaluate the recyclability of the TiO_2-BN nanocomposites under 3-hour UV light irradiation. Because the filtration and the centrifugation were not effective to collect all the nanocomposites from the solution, the suspensions were dried at 80 °C overnight after each degradation experiment to evaporate water from the ibuprofen and nanofibers mixture solution. Fresh ibuprofen solution was then added to the dried nanocomposites to repeat the photocatalytic experiment.

2.3 Analytical methods

The adsorption and degradation of ibuprofen were characterized by a high-performance liquid chromatography (HPLC; PerkinElmer Series 200, CT, USA), UV absorbance at 254 nm (UV_{254}), and dissolved organic carbon (DOC) quantified through a carbon analyzer (Shimadzu TOC-L, Kyoto, Japan). Specific UV absorbance (SUVA) was quantified by dividing the UV_{254} by the corresponding DOC concentration of ibuprofen samples, which indicates the change of aromatic

157 structure of ibuprofen molecules. Fluorescence excitation-emission matrix (FEEM) spectroscopy
158 was used to obtain information on characteristics of ibuprofen and potential degradation
159 products in water samples (Aqualog-UV-800-C; Horiba Instruments Inc., NJ).

160 The intermediate products of the ibuprofen degradation were further investigated using a (+) ESI
161 LC-MS/MS method with an Ultimate 3000 nano-flow LC system coupled to an Orbitrap Fusion
162 mass spectrometer equipped with an Adivon NanoMate nano-electrospray ionization source.
163 The LC solvent system consisted of water with 0.1% formic acid (A) and acetonitrile with 0.1%
164 formic acid (B). The gradient was 2% B at 0 min to 95% B at 60 min with a 10 min 95% B flush
165 and 20 min equilibration between samples. Data-dependent Orbitrap MS2 mass spectra (HCD
166 Energy = 27%, RP = 30000) were collected with a 3-sec cycle time between parent scans (m/z
167 100-1000, RP = 120000). Easy-IC lock mass calibration was used for parent scans. Background
168 ion signals were excluded from tandem mass spectrometry. Accurate mass measurement for
169 parent ions (e.g. <1 part per million, ppm) was used to constrain tandem mass spectral library
170 matching and impart high confidence to the matched results. Tandem mass spectra were searched
171 against the 2017 NIST tandem MS library and only matches within 1 ppm precursor mass
172 tolerance, 0.5 m/z product ion mass tolerance, a reverse match factor > 700, and C# < 13 were
173 considered robust matches.

174

175 2.4 Adsorption and photocatalytic kinetic models

176 Adsorption kinetics are usually governed by film diffusion and intra-particle diffusion (Lu Lin,
177 2014; Xuesong Xu, 2015; Lin et al., 2017g). However, the adsorption kinetics in this study are
178 complex due to the desorption of ibuprofen molecules from nanofibers with weak adsorption

bonding energy. Thus, the adsorption capacity and the rate to reach the equilibrium concentration were investigated using a commonly used kinetic model: the pseudo first-order kinetic model.

Typically, the performance of TiO_2 photocatalysis is usually characterized by Langmuir–Hinshelwood kinetic model (Turchi and Ollis, 1990; Ollis et al., 1991; Coleman et al., 2000; Tanaka et al., 2000; Houas et al., 2001; Li et al., 2006; Kumar and Devi, 2011b). It describes a pseudo-first-order kinetics when the initial concentration of ibuprofen is low (millimolar) (Houas et al., 2001; Konstantinou and Albanis, 2004) (Eq. 1):

$$ln\left(\frac{C_0}{C}\right) = k_{app}t \quad (1)$$

where C_0 and C are the initial and real-time ibuprofen concentrations (mg L^{-1}) at time t (min), k_{app} is the apparent pseudo-first-order rate constant (min^{-1}).

3. Results and discussion

3.1 Characterization of the synthesized catalysts

As shown in Figure 1, the peaks in XRD spectra were referred to primary anatase TiO_2 phase in the synthesized catalysts with presence of trace amount of rutile TiO_2 phase. Energy dispersive X-ray spectra (EDX) indicated the amounts of elements B and N increased with increasing BN dose in the TiO_2-BN nanocomposites (Nasr et al., 2017a). However, the XRD patterns of TiO_2-BN nanocomposites were similar to the pure TiO_2, suggesting the doping of BN had marginal impact on TiO_2 crystallization during electrospinning process.

199 The elemental mapping images revealed that Ti, O, B and N elements were evenly distributed
200 over the entire area of the synthesized materials (Nasr et al., 2017a). The morphological and
201 structural features of the synthesized materials were examined by TEM as shown in Figure S1.
202 The TiO_2-BN nanocomposites with different BN doses all displayed in a similar fiber form. The
203 crystallite size of the nanofibers can be determined by Scherrer equation (Lin et al., 2017e). The
204 crystallite sizes of the TiO_2-BN nanocomposites increased slightly with the increasing BN dose
205 (24.3-28.7 nm), while the particle size of pure TiO_2 was the smallest of 16.4 nm (Table 1). The
206 increasing trend of grain sizes was also observed by scanning electron microscopy (SEM)
207 images in previous study (Nasr et al., 2017a). This can be attributed to the increase of the
208 solution viscosity induced by inclusion of BN in the electrospinning solution (Nalbandian et al.,
209 2015). This increase revealed the successful incorporation of BN in TiO_2 nanofibers. Besides,
210 previous XPS analysis of TiO_2-BN nanocomposite suggested the formation of chemical B-O-Ti
211 bond between a titanium atom of TiO_2 and a boron atom at the edge of BN in TiO_2-BN
212 nanocomposite (Liu et al., 2017).

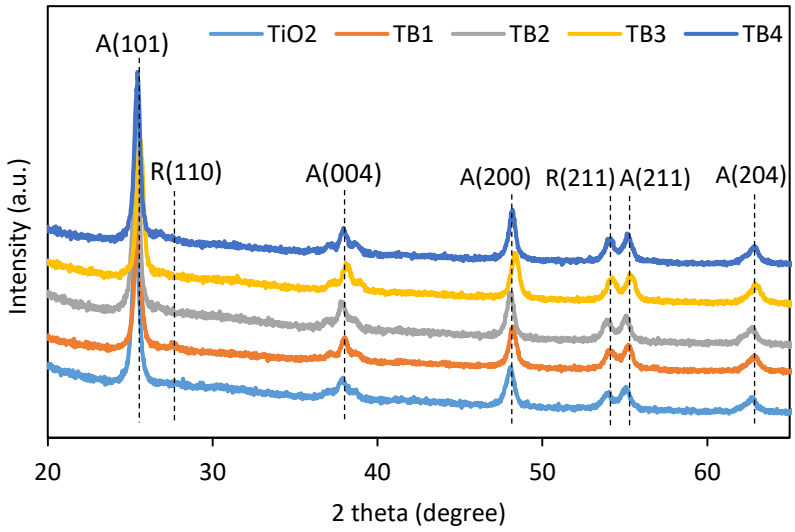

213

214 Figure 1. XRD patterns of synthesized catalysts. A: anatase; R: rutile.

The specific surface area of the synthesized nanocomposites increased from 19.7 m^2 g^{-1} to 49.6 m^2 g^{-1} with the increasing dose of BN nanosheets in the composites (Table 1). In general, materials with a large surface area can accelerate adsorption process due to more active adsorption sites available (Lin et al., 2017a). In addition, the UV-Vis absorption spectra of TiO_2, TB1, TB2, TB3, and TB4 measured in previous study (Nasr et al., 2017a) demonstrated that the incorporation of BN nanosheets improved the light absorbance of the TiO_2-BN nanocomposites in the range of 350-550 nm, which corresponds to the irradiance peak of the UV lamp used in the present work. As such, a higher photocatalytic performance could be expected by combining TiO_2 nanofibers with BN nanosheets. The increased light absorption efficiency resulted in an enhanced photocatalytic activity, which was further evidenced by the degradation of ibuprofen using TiO_2-BN nanocomposites in Section 3.3.

Table 1. Characterization of the synthesized nanocomposites

Photocatalysts	TiO_2	TB1	TB2	TB3	TB4
Specific surface area (m^2 g^{-1})	19.7	31.8	34.4	48.3	49.6
Crystalline size (nm)	16.4	24.3	25.2	26.3	28.7

3.2 Adsorption kinetics of the synthesized catalysts

The adsorption kinetics for ibuprofen onto different photocatalysts are shown in Figure 2. Ibuprofen molecules adsorbed onto photocatalysts from the aqueous solution increased quickly

over time, and the equilibrium was achieved within 90 min for all photocatalysts. Adsorption onto synthesized nanocomposites showed the same inverted "L" shape, indicating a similar kinetic adsorption process. The adsorption capacity of these catalysts varied in the range of 40-65% after 3-hour adsorption. Ibuprofen had better affinity and higher adsorption with pure TiO_2 than with TiO_2-BN nanocomposites.

The model parameters and the coefficients of determination (R^2) of the pseudo first-order kinetic equation were calculated based on the experimental data, and the results are summarized in Table 2 (modeling curves are presented in Supporting Information Figure S2). The kinetic model fitted well to the experimental data with the coefficients of determination (R^2) higher than 0.8. The amount of adsorbed ibuprofen at equilibrium (q_e) was approximately 14 mg g^{-1} for all nanocomposites, except for TB4 (10.3 mg g^{-1}). Pure TiO_2 achieved the highest adsorption kinetic rate constant (k_1 = 0.106 min^{-1}), which was 10 times larger than that of TB1. The adsorption kinetic rate constants followed the order of TiO_2 > TB2 > TB3 > TB4 > TB1, which was similar to the tendency observed in Figure 2.

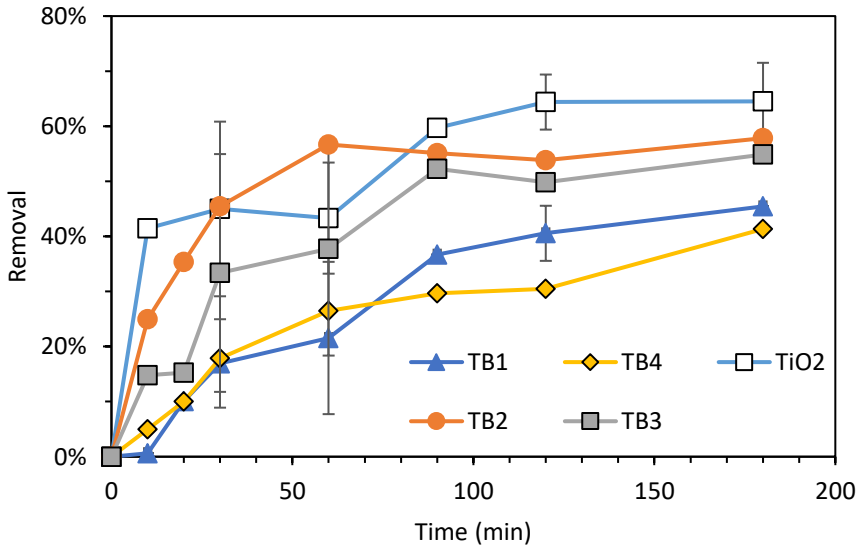

Figure 2. Adsorption kinetics of ibuprofen onto different photocatalysts. Error bars represent the standard deviation of duplicate experiments.

Generally, wrapping BN nanosheet onto TiO_2 nanofibers is expected to raise the ibuprofen adsorption onto the photocatalyst due to the larger specific surface area (Table 1). However, the interactions between ibuprofen and the nanocomposite catalysts also govern the adsorption process. Lee *et al.* proposed that the adsorption mechanism between TiO_2 and organics involved the electrostatic (H-bonding) and the covalent (bidentate-bridging mode) bonding (Lee et al., 2011). The surface complex was formed via H-bonding with TiOH/Ti-OH_2 (Ti-O) and COO- (COOH) groups (Lee et al., 2011). Besides, ibuprofen is negatively charged with the acid-base logarithmic ionization constant pK_a of 4.85 at neutral pH (Lin et al., 2017a). TiO_2 nanofibers are nearly neutral at pH 7 with the point of zero charge pH_{pzc} of 6.4, while the BN nanosheets are hydrophilic and negatively charged (Lin et al., 2010). As such, the introduction of BN increased the electrical repulsion between ibuprofen and the catalysts, resulting in lower adsorption. In addition, smaller particle size of pure TiO_2 (Table 1) may contribute to higher ibuprofen adsorption because smaller dimension often facilitates adsorption (Yean et al., 2005).

Table 2. Kinetic parameters for adsorption and photocatalytic activity of the pure TiO_2 and TiO_2-BN nanocomposites

Catalyst	Adsorption			Photocatalysis	
	k_1 (min^{-1})	q_e (mg g^{-1})	R^2	k_{app} (min^{-1})	R^2

TiO_2	0.106	14.13	0.836	0.047	0.994
TB1	0.010	13.95	0.974	0.028	0.985
TB2	0.052	14.1	0.996	0.033	0.979
TB3	0.024	13.77	0.964	0.041	0.975
TB4	0.015	10.28	0.974	0.054	0.952

267

268 3.3 Photocatalytic kinetics of the synthesized catalysts

269 The photodegradation of ibuprofen under UV irradiation is shown in Figure 3. The degradation
270 efficiency of direct photolysis (no catalyst) was measured under the same conditions for
271 photocatalysis (with catalyst). After 120 min of UV light exposure, there was 27% degradation
272 of ibuprofen without catalyst. It suggests that ibuprofen molecules can absorb UV light in the
273 region of lamp emission. On the other hand, photodegradation of ibuprofen remarkably improved
274 due to the enhancing effect of the nanocomposites under the UV irradiation. After 2 h of UV
275 light exposure, ibuprofen was almost completely degraded in the presence of photocatalysts.

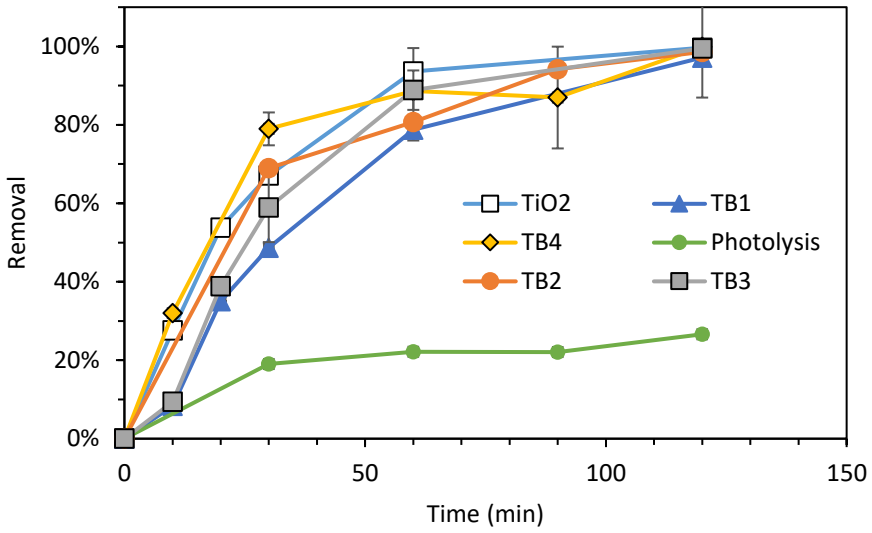

Figure 3. Photocatalytic kinetics of ibuprofen onto different photocatalysts under UV light irradiation. Error bars represent the standard deviation of duplicate experiments.

Langmuir-Hinshelwood kinetic model (Eq. 1) was applied to the photocatalytic data. A plot of $\ln(C_0/C)$ *versus* time t for ibuprofen degradation is presented in Figure 4, and the kinetic parameters are listed in Table 2. The Langmuir–Hinshelwood kinetic model fitted well the experimental data and the coefficients of determination (R^2) obtained were greater than 0.9. The photocatalytic activity presented a similar trend as BN content, except for pure TiO_2. As shown in Table 2, the apparent photocatalysis rate of TB4 (0.054 min^{-1}) was higher than pure TiO_2 (0.047 min^{-1}), while TiO_2 had higher adsorption kinetics rate (TiO_2 0.059 vs. TB4 0.039 min^{-1}). Hence, TB4 exhibits excellent photocatalytic activity for ibuprofen removal rather than adsorption. The photocatalytic degradation rates of TiO_2 and TB2 were lower than adsorption rates, inferring that their adsorption rate is faster than the photocatalytic oxidation rate, so oxidation is the control step for the photocatalytic reaction. On the contrary, adsorption is the

control step for TB1, TB3, and TB4 photocatalysis. This was further demonstrated by the multiple photocatalysis cycles discussed in Section 3.6.

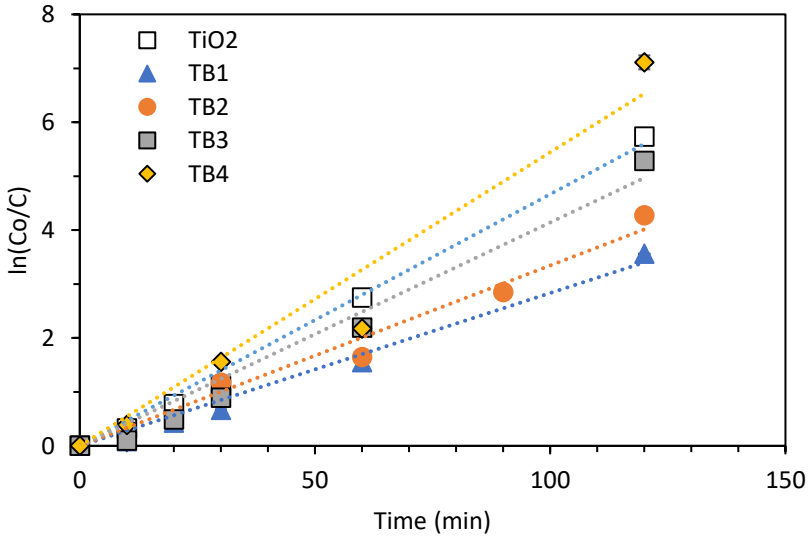

Figure 4. Langmuir-Hinshelwood kinetic modeling curves of ibuprofen degradation by the synthesized nanocomposites

Adsorption has both positive and negative impacts on photocatalysis. On the one hand, more adsorbed ibuprofen molecules on the catalyst surface improve the transfer of photogenerated radicals, which explained why the photocatalytic degradation rate of TiO_2 was slightly higher than TB1 and TB2. On the other hand, the photocatalytic activity is mainly affected by light absorption capacity and separation efficiency of e^--h^+ pairs. The adsorbed ibuprofen may hinder the photocatalysis degradation by screening the light access to the catalysis, so photocatalytic degradation rate of TiO_2 was relatively low even with the highest adsorption rate. The photocatalytic degradation rate of TiO_2-BN nanocomposite increased with the increasinng BN content probably due to enhanced light absorption intensity (Section 3.1). Meanwhile, due to

306 electrostatic interactions, the negatively charged BN nanosheets surface can lead to the transfer
307 of h^+ from the TiO_2 particles to the BN nanosheets. As such, the recombination of e^- and h^+ is
308 inhibited with increasing BN dose, which was confirmed by previous photoluminescence study
309 (Nasr et al., 2017a).

310

311 3.4 Ibuprofen degradation intermediates and proposed pathway

312 Aiming at identifying the degradation intermediates, (+) ESI LC-MS/MS was performed to
313 detect the constituents in the ibuprofen solutions after photocatalytic treatment. Figure 5 showed
314 extracted-ion chromatographic peak areas for ibuprofen degradation intermediates (including
315 hydroxyibuprofen, carboxyibuprofen, and oxypropyl ibuprofen) after 2-hour UV irradiation. The
316 proposed photocatalytic degradation pathway of ibuprofen is present in Figure 6. All compounds
317 shown were confirmed by high resolution mass spectrometry, where elemental composition of
318 the parent ions was determined from accurate m/z measurement and tandem mass spectrometry
319 indicates molecular structure. For simplicity, only one isomer among several possible is shown at
320 each step. Some intermediates are proposed to be formed by successive free radical
321 hydroxylation followed by oxidation to yield the carbonyl compounds (aldehyde and ketone).
322 The primary carbon oxidation to carboxylic acid is a facile process and that product is confirmed
323 by our mass spectrometry results. The most reactive site of the ibuprofen molecule in the
324 presence of free radical ($^{\bullet}OH$) is the benzylic carbon, which gives monohydroxylated ibuprofen
325 (confirmed by mass spectrometry). Once the benzylic hydroxyl ibuprofen is formed, it undergoes
326 further oxidation to give the beta-keto acid. Beta keto acids are susceptible for decarboxylation
327 and results the formation of oxypropyl ibuprofen. A similar oxidation decarboxylation route for
328 the degradation of ibuprofen has been reported in the literature (Skoumal et al., 2009).

As presented in Figure 3, the sample under direct photolysis (no catalyst) displayed the lowest removal of ibuprofen (27% in 2-hour UV irradiation) and relatively low amounts of degradation intermediates (Figure 5). It suggested only a small fraction of ibuprofen was oxidized and the degradation process was limited to the initial degradation levels. Degradation in the existence of photocatalysts is more complete since both ibuprofen and its degradation products can be adsorbed onto the catalysts. From Figure 3, ibuprofen was almost completely degraded in the presence of photocatalysts after 2-hour UV light exposure, but the amounts of degradation intermediates varied remarkably (Figure 5). Comparing to direct photolysis, the pure TiO_2 catalyst showed 27 times, 12 times, and 76 times increase in hydroxyibuprofen, carboxyibuprofen, and oxypropyl ibuprofen, respectively, owing to the degradation of parent compound (ibuprofen). When the BN content increased to 3% (TB1), the amount of degradation intermediates showed 4%, 60%, and 28% reduction relative to the pure TiO_2. The catalysts with 5% BN (TB2) also showed a similar increase in degradation intermediates. However, when the BN content increased to 7% (TB3) and 10% (TB4), the degradation intermediates decreased by over 99%, 99%, and 90% for hydroxyibuprofen, carboxyibuprofen, and oxypropyl ibuprofen, respectively, comparing to the pure TiO_2. Hence, the increasing BN content of the catalyst facilitated the breakdown of ibuprofen degradation intermediates. However, the further degradation products were not detected with (+) ESI LC-MS/MS probably due to the low concentration of these compounds. These degradation products with smaller carbon chains might be adsorbed onto the catalysts surface and degraded much faster than ibuprofen and its initial degradation intermediates. More analysis of degradation mechanism was discussed in the following Section 3.5.

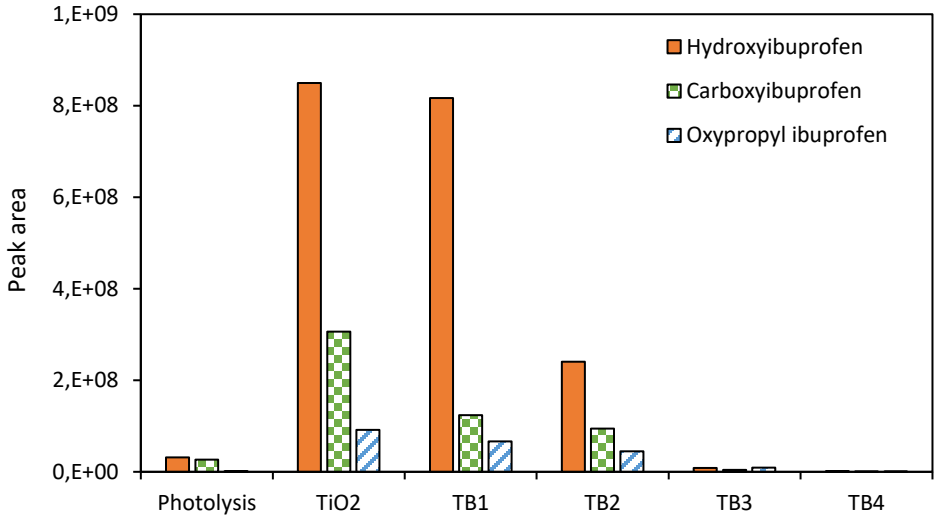

351

352 Figure 5. Extracted-ion chromatographic peak areas for the precursor masses of ibuprofen
353 degradation intermediates derived from (+) ESI LC-MS/MS chromatograms from different
354 catalyst conditions.

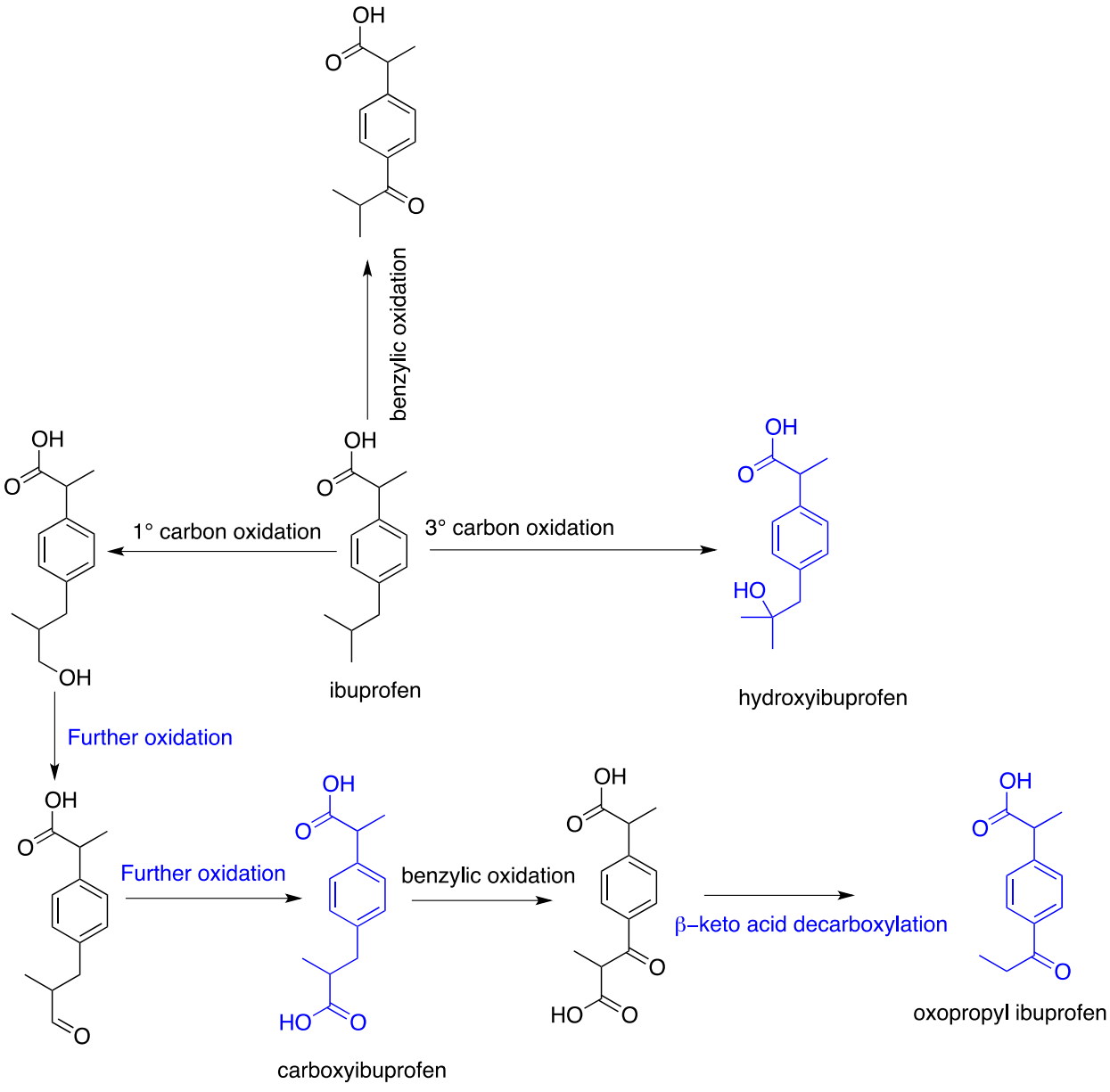

355

356 Figure 6. Proposed degradation of ibuprofen by TiO_2-BN photocatalysis. Indicated structures

357 were confirmed by mass spectrometry as described.

358

3.5 Photocatalytic oxidation mechanisms of ibuprofen

The nanocomposite TB4 was chosen to investigate the photocatalytic degradation mechanism of ibuprofen because of its highest photocatalytic activity among the TiO_2-BN nanocomposites. The photodegradation of ibuprofen was analyzed in terms of HPLC, FEEM, DOC, UV_{254}, and SUVA measurements (Figure 7). The concentration measured by HPLC was the exact concentration of ibuprofen (parent compound); its concentration reduced rapidly and almost completely disappeared after 2-hour reaction. DOC includes all organic carbons in parent compounds, degradation intermediates and products, serving as an indicator for mineralization degree. Compared with the ibuprofen removal results from the HPLC analysis, the DOC reduction was much slower, with only 25% after 2-h reaction. Although the TB4 was effective to oxidize ibuprofen at a fast rate, the organic intermediates from the ibuprofen oxidation need longer time to be mineralized.

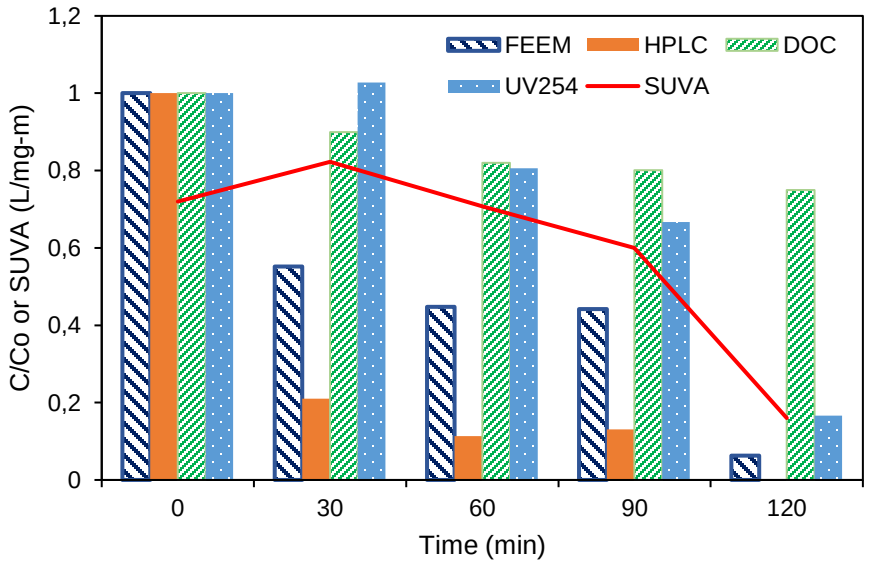

Figure 7. Reduction of DOC, FEEM peak values, and SUVA values during photocatalytic oxidation of ibuprofen using TB4 under UV irradiation

The UV_{254} and SUVA are used to determine the removal of aromatic fractions of ibuprofen (Stoll et al., 2015). As shown in Figure 7, the SUVA and UV_{254} results exhibited a similar removal trend suggesting aromatic fraction of ibuprofen was degraded. Even though ibuprofen concentration reduced by 79% for the first 30 min, there were 14% and 3% increases in terms of SUVA and UV_{254}, respectively. The degradation of ibuprofen was further characterized by the FEEM spectroscopy. The fluorescence peak disappeared after 2-hour of treatment (Figure S3). The excitation-emission peak observed at 220 nm/285 nm corresponds to aromatic compounds (Chen et al., 2003). The fluorescence peak volume was used to compare the aromatic fractions in the tested ibuprofen solution at different reaction time (Figure 7). The peak volume reduced by 94% after 2-hour reaction, supporting the decrease in aromatic compounds, consistent with the results of UV_{254} and SUVA that aromatic organic carbon was removed from the solution.

The results implied that the intermediates become more aromatic than the parent compound after a partial oxidation. As discussed in Section 3.4, intermediates with more complex structure were detected after photocatalytic treatment. Interestingly, there was only 13% reduction of ibuprofen concentration in the last 30 min of reaction (from 90 to 120 min), but SUVA, UV_{254}, and FEEM decreased by 61%, 50%, and 38%, respectively. It suggested that decomposition from parent compounds to intermediates happened mainly during the initial 90 min, while degradation of intermediates into shorter carbon chains occurred mainly after decomposition. Besides, the DOC reduction in the first 30 min probably attributed to the adsorption of ibuprofen onto TB4 (Figure 3), the mineralization of ibuprofen was a slow process in the following 90 min due to the tardy reduction of DOC. These results demonstrated that photocatalytic oxidation of ibuprofen

molecules by the synthesized nanofibers is a complex multi-step process, degradation of intermediates is probably a control step for the ibuprofen photocatalytic oxidation.

3.6 Recyclability of the synthesized catalysts

The recyclability of the photocatalysts by reusing the catalysts in multiple treatment cycles is crucial in accessing the practical application of a catalyst, because the catalyst may be poisoned by some species (e.g., reaction intermediates) during the reaction process, or may otherwise decompose. In the present work, the recyclability of the pure TiO_2 and TB4 was investigated by performing 16 UV irradiation cycles. In each cycle, UV light was irradiated for 3-hour at room temperature. The adsorption of ibuprofen by TiO_2 and TB4 achieved 65% and 41% after 3-hour mixing (Figure 2), but the photocatalytic activity of TiO_2 and TB4 still remained 80% and 79% after eight cycles of photocatalytic reaction (Figure 8).

After eight cycles, the used nanofibers were irradiated by the UV lamp for 3-hour in deionized water. The treatment efficiency was recovered to 98% and 95% for TB4 and TiO_2 after 3-hour regeneration by UV irradiation. However, the degradation efficiency of ibuprofen receded gradually in the following eight cycles, although the TB4 remarkably outperformed TiO_2. According to Section 3.4, more ibuprofen and intermediates were detected for TiO_2 than TB4, hence, weaker photocatalytic activity is probably attributed to the generation and accumulation of intermediates during the catalytic process, which remained on the catalyst and may restrain the further adsorption and degradation of ibuprofen. In addition to the UV irradiation as an effective method for the regeneration of exhausted nanofibers, chemical regeneration should also be studied to fully restore the photocatalysts.

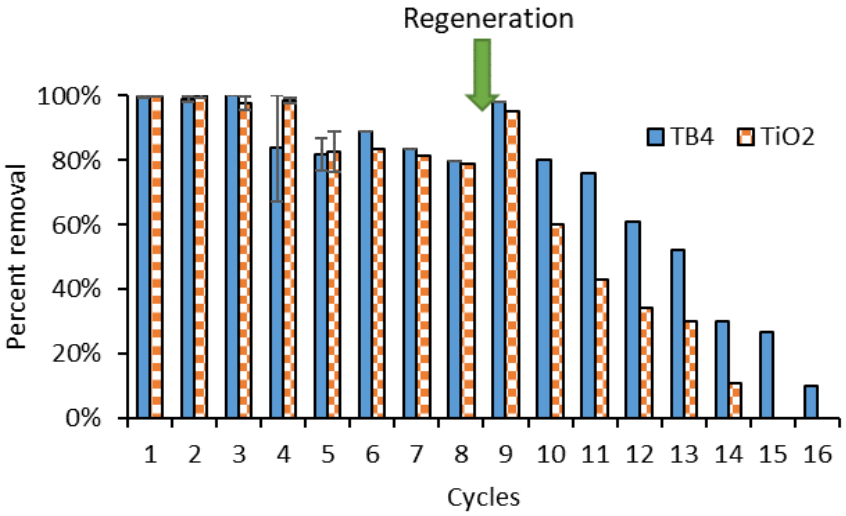

Figure 8. Ibuprofen removal efficiency of TB4 and TiO_2 catalysts during multiple photocatalytic cycles under the irradiation of UV light

4. Conclusions

The adsorption, photolysis, and photocatalytic oxidation of ibuprofen by TiO_2-BN nanocomposites were studied using a multiple analysis approach. The degradation kinetics, mechanisms, and intermediate products were elucidated. The primary conclusions of the study are summarized as follows.

- Wrapping BN nanosheets onto TiO_2 nanofibers improved light absorption efficiency and specific surface area of TiO_2 nanofibers, and enhanced separation effectiveness of photogenerated e^--h^+ pairs.
- Both adsorption and photocatalytic oxidation of ibuprofen by the TiO_2-BN nanocomposites followed the first-order kinetic models. The amount of adsorbed ibuprofen at

equilibrium reached approximately 14 mg g^{-1} for the TiO_2-BN photocatalysts. The photocatalytic degradation rate increased with the increasing BN content.

- Analysis of degradation intermediates suggested that the increasing BN content of the catalyst facilitated the breakdown of ibuprofen degradation intermediates (hydroxyibuprofen, carboxyibuprofen, and oxypropyl ibuprofen). No further degradation intermediates were detected by the (+) ESI LC-MS/MS chromatograms likely due to lower concentrations of these compounds.
- Multiple photocatalytic cycles were conducted to investigate the reusability of the photocatalysts. UV irradiation of the catalysts in clean water could recover the degradation efficiency to 98% and 95% for TB4 and TiO_2. However, photocatalytic activity receded gradually, especially TiO_2, as a result of the accumulation of intermediates during the catalytic process. Further chemical regeneration should be investigated to fully recover the photocatalysts.
- Combining TiO_2 nanofibers with BN nanosheets provides an innovative method to improve the photocatalytic performance for the degradation of organic contaminants. Further studies on photocatalytic oxidation of organic contaminants of emerging concerns should be conducted using solar light in environmental conditions (e.g., wastewater).

Acknowledgments

Support for this study was provided by the United States National Science Foundation (NSF) Engineering Research Center Program under Cooperative Agreement EEC-1028968 (ReNUWIt); and National Science Foundation Major Research Instrumentation Program (NSF MRI 1626468).

454

References

Andreozzi, R., Caprio, V., Insola, A., Marotta, R., 1999. Advanced oxidation processes (AOP) for water purification and recovery. Catalysis Today 53, 51-59.

Arlos, M.J., Liang, R., Hatat-Fraile, M.M., Bragg, L.M., Zhou, N.Y., Servos, M.R., Andrews, S.A., 2016. Photocatalytic decomposition of selected estrogens and their estrogenic activity by UV-LED irradiated TiO2 immobilized on porous titanium sheets via thermal-chemical oxidation. J Hazard Mater 318, 541-550.

Asiltürk, M., Sayılkan, F., Arpaç, E., 2009. Effect of Fe3+ ion doping to TiO2 on the photocatalytic degradation of Malachite Green dye under UV and vis-irradiation. Journal of Photochemistry and Photobiology A: Chemistry 203, 64-71.

Bauer, C., Jacques, P., Kalt, A., 2001. Photooxidation of an azo dye induced by visible light incident on the surface of TiO 2. Journal of Photochemistry and Photobiology A: Chemistry 140, 87-92.

Biscarat, J., Bechelany, M., Pochat-Bohatier, C., Miele, P., 2015. Graphene-like BN/gelatin nanobiocomposites for gas barrier applications. Nanoscale 7, 613-618.

Blake, D., 2001. Bibliography of Work on the Heterogeneous Photocatalytic Removal of Hazardous Compounds from Water and Air--Update Number 4 to October 2001. National Renewable Energy Lab., Golden, CO (US).

Carbonaro, S., Sugihara, M.N., Strathmann, T.J., 2013. Continuous-flow photocatalytic treatment of pharmaceutical micropollutants: Activity, inhibition, and deactivation of TiO2 photocatalysts in wastewater effluent. Applied Catalysis B: Environmental 129, 1-12.

Chen, W., Westerhoff, P., Leenheer, J.A., Booksh, K., 2003. Fluorescence Excitation−Emission Matrix Regional Integration to Quantify Spectra for Dissolved Organic Matter. Environmental Science & Technology 37, 5701-5710.

Christen, V., Hickmann, S., Rechenberg, B., Fent, K., 2010. Highly active human pharmaceuticals in aquatic systems: A concept for their identification based on their mode of action. Aquatic Toxicology 96, 167-181.

Coleman, H.M., Eggins, B.R., Byrne, J.A., Palmer, F.L., King, E., 2000. Photocatalytic degradation of 17-β-oestradiol on immobilised TiO2. Appl. Catal., B 24, L1-L5.

Dalrymple, O.K., Yeh, D.H., Trotz, M.A., 2007. Removing pharmaceuticals and endocrine-disrupting compounds from wastewater by photocatalysis. Journal of Chemical Technology & Biotechnology 82, 121-134.

De la Cruz, N., Giménez, J., Esplugas, S., Grandjean, D., De Alencastro, L., Pulgarin, C., 2012. Degradation of 32 emergent contaminants by UV and neutral photo-fenton in domestic wastewater effluent previously treated by activated sludge. water research 46, 1947-1957.

De Witte, B., Dewulf, J., Demeestere, K., Van Langenhove, H., 2009. Ozonation and advanced oxidation by the peroxone process of ciprofloxacin in water. Journal of Hazardous Materials 161, 701-708.

Doll, T.E., Frimmel, F.H., 2004. Kinetic study of photocatalytic degradation of carbamazepine, clofibric acid, iomeprol and iopromide assisted by different TiO2 materials—determination of intermediates and reaction pathways. Water Research 38, 955-964.

Fujishima, A., Rao, T.N., Tryk, D.A., 2000. Titanium dioxide photocatalysis. Journal of Photochemistry and Photobiology C: Photochemistry Reviews 1, 1-21.

Harifi, T., Montazer, M., 2014. Fe3+:Ag/TiO2 nanocomposite: Synthesis, characterization and photocatalytic activity under UV and visible light irradiation. Applied Catalysis A: General 473, 104-115.

Homem, V., Santos, L., 2011. Degradation and removal methods of antibiotics from aqueous matrices – A review. Journal of Environmental Management 92, 2304-2347.

Houas, A., Lachheb, H., Ksibi, M., Elaloui, E., Guillard, C., Herrmann, J.-M., 2001. Photocatalytic degradation pathway of methylene blue in water. Appl. Catal., B 31, 145-157.
Hu, C., Tang, Y., Jimmy, C.Y., Wong, P.K., 2003. Photocatalytic degradation of cationic blue X-GRL adsorbed on TiO 2/SiO 2 photocatalyst. Applied Catalysis B: Environmental 40, 131-140.
Huerta-Fontela, M., Galceran, M.T., Ventura, F., 2011. Occurrence and removal of pharmaceuticals and hormones through drinking water treatment. Water Research 45, 1432-1442.
Jing, L., Qu, Y., Wang, B., Li, S., Jiang, B., Yang, L., Fu, W., Fu, H., Sun, J., 2006. Review of photoluminescence performance of nano-sized semiconductor materials and its relationships with photocatalytic activity. Solar Energy Materials and Solar Cells 90, 1773-1787.
Konstantinou, I.K., Albanis, T.A., 2004. TiO2-assisted photocatalytic degradation of azo dyes in aqueous solution: kinetic and mechanistic investigations. Applied Catalysis B: Environmental 49, 1-14.
Kormann, C., Bahnemann, D., Hoffmann, M.R., 1991. Photolysis of chloroform and other organic molecules in aqueous titanium dioxide suspensions. Environmental science & technology 25, 494-500.
Kumar, S.G., Devi, L.G., 2011a. Review on modified TiO2 photocatalysis under UV/visible light: selected results and related mechanisms on interfacial charge carrier transfer dynamics. J Phys Chem A 115, 13211-13241.
Kumar, S.G., Devi, L.G., 2011b. Review on modified TiO2 photocatalysis under UV/visible light: selected results and related mechanisms on interfacial charge carrier transfer dynamics. J. Photochem. Photobiol., A 115, 13211-13241.
Le-Clech, P., Lee, E.-K., Chen, V., 2006. Hybrid photocatalysis/membrane treatment for surface waters containing low concentrations of natural organic matters. Water Research 40, 323-330.
Lee, C.-R., Kim, H.-S., Jang, I.-H., Im, J.-H., Park, N.-G., 2011. Pseudo First-Order Adsorption Kinetics of N719 Dye on TiO2 Surface. ACS Applied Materials & Interfaces 3, 1953-1957.
Lee, Y., von Gunten, U., 2010. Oxidative transformation of micropollutants during municipal wastewater treatment: Comparison of kinetic aspects of selective (chlorine, chlorine dioxide, ferrateVI, and ozone) and non-selective oxidants (hydroxyl radical). Water Research 44, 555-566.
Li, S., Hu, J., 2018. Transformation products formation of ciprofloxacin in UVA/LED and UVA/LED/TiO2 systems: Impact of natural organic matter characteristics. Water Res 132, 320-330.
Li, Y., Li, X., Li, J., Yin, J., 2006. Photocatalytic degradation of methyl orange by TiO2-coated activated carbon and kinetic study. Water Res. 40, 1119-1126.
Lin, L., Jiang, W., Xu, P., 2017a. Comparative study on pharmaceuticals adsorption in reclaimed water desalination concentrate using biochar: Impact of salts and organic matter. Sci Total Environ 601-602, 857-864.
Lin, L., Wang, H., Jiang, W., Mkaouar, A.R., Xu, P., 2017b. Comparison study on photocatalytic oxidation of pharmaceuticals by TiO2-Fe and TiO2-reduced graphene oxide nanocomposites immobilized on optical fibers. J Hazard Mater 333, 162-168.
Lin, L., Wang, H., Jiang, W., Mkaouar, A.R., Xu, P., 2017c. Comparison study on photocatalytic oxidation of pharmaceuticals by TiO 2-Fe and TiO 2-reduced graphene oxide nanocomposites immobilized on optical fibers. Journal of Hazardous Materials 333, 162-168.
Lin, L., Wang, H., Luo, H., Xu, P., 2015. Enhanced photocatalysis using side-glowing optical fibers coated with Fe-doped TiO2 nanocomposite thin films. Journal of Photochemistry and Photobiology A: Chemistry 307-308, 88-98.
Lin, L., Wang, H., Luo, H., Xu, P., 2016. Photocatalytic Treatment of Desalination Concentrate Using Optical Fibers Coated With Nanostructured Thin Films: Impact of Water Chemistry and Seasonal Climate Variations. Photochem Photobiol 92, 379-387.
Lin, L., Wang, H., Xu, P., 2017d. Immobilized TiO2-reduced graphene oxide nanocomposites on optical fibers as high performance photocatalysts for degradation of pharmaceuticals. Chemical Engineering Journal 310, Part 2, 389-398.

548 Lin, L., Wang, H., Xu, P., 2017e. Immobilized TiO 2-reduced graphene oxide nanocomposites on optical
549 fibers as high performance photocatalysts for degradation of pharmaceuticals. Chemical Engineering
550 Journal 310, 389-398.
551 Lin, L., Wang, H., Xu, P., 2017f. Immobilized TiO 2 -reduced graphene oxide nanocomposites on optical
552 fibers as high performance photocatalysts for degradation of pharmaceuticals. Chemical Engineering
553 Journal 310, 389-398.
554 Lin, L., Xu, X., Papelis, C., Xu, P., 2017g. Innovative use of drinking water treatment solids for heavy
555 metals removal from desalination concentrate: Synergistic effect of salts and natural organic matter.
556 Chemical Engineering Research and Design 120, 231-239.
557 Lin, Y., Williams, T.V., Connell, J.W., 2010. Soluble, Exfoliated Hexagonal Boron Nitride Nanosheets. The
558 Journal of Physical Chemistry Letters 1, 277-283.
559 Liqiang, J., Yichun, Q., Baiqi, W., Shudan, L., Baojiang, J., Libin, Y., Wei, F., Honggang, F., Jiazhong, S.,
560 2006. Review of photoluminescence performance of nano-sized semiconductor materials and its
561 relationships with photocatalytic activity. Solar Energy Materials and Solar Cells 90, 1773-1787.
562 Liu, D., Zhang, M., Xie, W., Sun, L., Chen, Y., Lei, W., 2017. Porous BN/TiO2 hybrid nanosheets as highly
563 efficient visible-light-driven photocatalysts. Applied Catalysis B: Environmental 207, 72-78.
564 Lu Lin, X.X., Charalambos Papelis, Tzahi Y. Cath, Pei Xu, 2014. Sorption of metals and metalloids from
565 reverse osmosis concentrate on drinking water treatment solids. Separation and Purification Technology
566 134, 37-45.
567 Lv, Y., Cao, X., Jiang, H., Song, W., Chen, C., Zhao, J., 2016. Rapid photocatalytic debromination on TiO2
568 with in-situ formed copper co-catalyst: Enhanced adsorption and visible light activity. Applied Catalysis B:
569 Environmental 194, 150-156.
570 Merenda, A., Kong, L., Zhu, B., Duke, M.C., Gray, S.R., Dumée, L.F., 2019. Functional Nanoporous
571 Titanium Dioxide for Separation Applications: Synthesis Routes and Properties to Performance Analysis.
572 in: Pannirselvam, M., Shu, L., Griffin, G., Philip, L., Natarajan, A., Hussain, S. (Eds.). Water Scarcity and
573 Ways to Reduce the Impact: Management Strategies and Technologies for Zero Liquid Discharge and
574 Future Smart Cities. Springer International Publishing, Cham, pp. 151-186.
575 Nakajima, T., Xu, Y.-H., Mori, Y., Kishita, M., Takanashi, H., Maeda, S., Ohki, A., 2005. Combined use of
576 photocatalyst and adsorbent for the removal of inorganic arsenic (III) and organoarsenic compounds
577 from aqueous media. Journal of hazardous materials 120, 75-80.
578 Nakata, K., Fujishima, A., 2012. TiO2 photocatalysis: Design and applications. Journal of Photochemistry
579 and Photobiology C: Photochemistry Reviews 13, 169-189.
580 Nalbandian, M.J., Zhang, M., Sanchez, J., Kim, S., Choa, Y.-H., Cwiertny, D.M., Myung, N.V., 2015.
581 Synthesis and optimization of Ag–TiO 2 composite nanofibers for photocatalytic treatment of impaired
582 water sources. Journal of hazardous materials 299, 141-148.
583 Nasr, M., Viter, R., Eid, C., Habchi, R., Miele, P., Bechelany, M., 2017a. Enhanced photocatalytic
584 performance of novel electrospun BN/TiO2composite nanofibers. New J. Chem. 41, 81-89.
585 Nasr, M., Viter, R., Eid, C., Habchi, R., Miele, P., Bechelany, M., 2017b. Enhanced photocatalytic
586 performance of novel electrospun BN/TiO 2 composite nanofibers. New Journal of Chemistry 41, 81-89.
587 Ollis, D.F., Hsiao, C.-Y., Budiman, L., Lee, C.-L., 1984. Heterogeneous photoassisted catalysis: conversions
588 of perchloroethylene, dichloroethane, chloroacetic acids, and chlorobenzenes. Journal of catalysis 88,
589 89-96.
590 Ollis, D.F., Pelizzetti, E., Serpone, N., 1991. Photocatalyzed destruction of water contaminants. Environ.
591 Sci. Technol. 25, 1522-1529.
592 Prieto-Rodriguez, L., Miralles-Cuevas, S., Oller, I., Agüera, A., Puma, G.L., Malato, S., 2012. Treatment of
593 emerging contaminants in wastewater treatment plants (WWTP) effluents by solar photocatalysis using
594 low TiO2 concentrations. Journal of Hazardous Materials 211, 131-137.

595 Rioja, N., Benguria, P., Peñas, F., Zorita, S., 2014. Competitive removal of pharmaceuticals from
596 environmental waters by adsorption and photocatalytic degradation. Environmental Science and
597 Pollution Research 21, 11168-11177.
598 Rosenfeldt, E.J., Linden, K.G., 2004. Degradation of Endocrine Disrupting Chemicals Bisphenol A, Ethinyl
599 Estradiol, and Estradiol during UV Photolysis and Advanced Oxidation Processes. Environmental Science
600 & Technology 38, 5476-5483.
601 Rubio, D., Casanueva, J.F., Nebot, E., 2013. Improving UV seawater disinfection with immobilized TiO2:
602 Study of the viability of photocatalysis (UV254/TiO2) as seawater disinfection technology. Journal of
603 Photochemistry and Photobiology A: Chemistry 271, 16-23.
604 Skoumal, M., Rodríguez, R.M., Cabot, P.L., Centellas, F., Garrido, J.A., Arias, C., Brillas, E., 2009. Electro-
605 Fenton, UVA photoelectro-Fenton and solar photoelectro-Fenton degradation of the drug ibuprofen in
606 acid aqueous medium using platinum and boron-doped diamond anodes. Electrochimica Acta 54, 2077-
607 2085.
608 Stoll, Z.A., Forrestal, C., Ren, Z.J., Xu, P., 2015. Shale gas produced water treatment using innovative
609 microbial capacitive desalination cell. J Hazard Mater 283, 847-855.
610 Tanaka, K., Padermpole, K., Hisanaga, T., 2000. Photocatalytic degradation of commercial azo dyes.
611 Water Res. 34, 327-333.
612 Tawkaew, S., Supothina, S., 2008. Preparation of agglomerated particles of TiO2 and silica-coated
613 magnetic particle. Materials Chemistry and Physics 108, 147-153.
614 Thagard, S.M., Stratton, G.R., Dai, F., Bellona, C.L., Holsen, T.M., Bohl, D.G., Paek, E., Dickenson, E.R.,
615 2016. Plasma-based water treatment: development of a general mechanistic model to estimate the
616 treatability of different types of contaminants. Journal of Physics D: Applied Physics 50, 014003.
617 Turchi, C.S., Ollis, D.F., 1990. Photocatalytic degradation of organic water contaminants: Mechanisms
618 involving hydroxyl radical attack. J. Catal. 122, 178-192.
619 Van Doorslaer, X., Dewulf, J., De Maerschalk, J., Van Langenhove, H., Demeestere, K., 2015.
620 Heterogeneous photocatalysis of moxifloxacin in hospital effluent: Effect of selected matrix constituents.
621 Chemical Engineering Journal 261, 9-16.
622 Vautier, M., Guillard, C., Herrmann, J.-M., 2001. Photocatalytic degradation of dyes in water: case study
623 of indigo and of indigo carmine. Journal of Catalysis 201, 46-59.
624 Vieno, N.M., Härkki, H., Tuhkanen, T., Kronberg, L., 2007. Occurrence of Pharmaceuticals in River Water
625 and Their Elimination in a Pilot-Scale Drinking Water Treatment Plant. Environmental Science &
626 Technology 41, 5077-5084.
627 Wang, H., Heil, D., Ren, Z.J., Xu, P., 2015. Removal and fate of trace organic compounds in microbial fuel
628 cells. Chemosphere 125, 94-101.
629 Westerhoff, P., Yoon, Y., Snyder, S., Wert, E., 2005. Fate of endocrine-disruptor, pharmaceutical, and
630 personal care product chemicals during simulated drinking water treatment processes. Environmental
631 science & technology 39, 6649-6663.
632 Wold, A., 1993. Photocatalytic properties of titanium dioxide (TiO2). Chemistry of Materials 5, 280-283.
633 Xiang, Y., Fang, J., Shang, C., 2016. Kinetics and pathways of ibuprofen degradation by the UV/chlorine
634 advanced oxidation process. Water Res 90, 301-308.
635 Xuesong Xu, L.L., Charalambos Papelis, Maung Myint, Tzahi Y. Cath, Pei Xu, 2015. Use of drinking water
636 treatment solids for arsenate removal from desalination concentrate. Journal of Colloid and Interface
637 Science 455, 252-261.
638 Yean, S., Cong, L., Yavuz, C., Mayo, J., Yu, W., Kan, A., Colvin, V., Tomson, M., 2005. Effect of magnetite
639 particle size on adsorption and desorption of arsenite and arsenate. Journal of Materials Research 20,
640 3255-3264.
641 Yi, Z., Merenda, A., Kong, L., Radenovic, A., Majumder, M., Dumée, L.F., 2018. Single step synthesis of
642 Schottky-like hybrid graphene - titania interfaces for efficient photocatalysis. Scientific Reports 8, 8154.

643 Yu, Y., Yu, J.C., Chan, C.-Y., Che, Y.-K., Zhao, J.-C., Ding, L., Ge, W.-K., Wong, P.-K., 2005. Enhancement of
644 adsorption and photocatalytic activity of TiO2 by using carbon nanotubes for the treatment of azo dye.
645 Applied Catalysis B: Environmental 61, 1-11.
646 Zhang, S., Chen, L., Liu, H., Guo, W., Yang, Y., Guo, Y., Huo, M., 2012. Design of H3PW12O40/TiO2 and
647 Ag/H3PW12O40/TiO2 film-coated optical fiber photoreactor for the degradation of aqueous rhodamine
648 B and 4-nitrophenol under simulated sunlight irradiation. Chemical Engineering Journal 200-202, 300-
649 309.
650 Zhang, Z., Xiao, F., Guo, Y., Wang, S., Liu, Y., 2013. One-pot self-assembled three-dimensional TiO2-
651 graphene hydrogel with improved adsorption capacities and photocatalytic and electrochemical
652 activities. ACS Appl Mater Interfaces 5, 2227-2233.

653

654

List of the Figure Captions

Figure 1. XRD patterns of synthesized catalysts. A: anatase; R: rutile.

Figure 2. Adsorption kinetics of ibuprofen onto different photocatalysts. Error bars represent the standard deviation of duplicate experiments.

Figure 3. Photocatalytic kinetics of ibuprofen onto different photocatalysts under UV light irradiation. Error bars represent the standard deviation of duplicate experiments.

Figure 4. Langmuir-Hinshelwood kinetic modeling curves of ibuprofen degradation by the synthesized nanocomposites

Figure 5. Extracted-ion chromatographic peak areas for the precursor masses of ibuprofen degradation intermediates derived from (+) ESI LC-MS/MS chromatograms from different catalyst conditions.

Figure 6. Proposed degradation of ibuprofen by TiO_2-BN photocatalysis. Indicated structures were confirmed by mass spectrometry as described.

Figure 7. Reduction of DOC, FEEM peak values, and SUVA values during photocatalytic oxidation of ibuprofen using TB4 under UV irradiation

Figure 8. Ibuprofen removal efficiency of TB4 and TiO_2 catalysts during multiple photocatalytic cycles under the irradiation of UV light